ACS Sustainable Chemistry & Engineering

Research Article

pubs.acs.org/journal/ascecg

Application for Simply Recovered $LiCoO_2$ Material as a High-Performance Candidate for Supercapacitor in Aqueous System

Yanan Xu,[†] Yanying Dong,[†] Xiao Han,[‡] Xiaofeng Wang,[†] Yijing Wang,*[,†] Lifang Jiao,[†] and Huatang Yuan[†]

[†]College of Chemistry, Collaborative Innovation Center of Chemical Science and Engineering (Tianjin), Key Laboratory of Advanced Energy Materials Chemistry (MOE), Tianjin Key Lab of Metal and Molecule-based Material Chemistry, Nankai University, Tianjin 300071, People's Republic of China

[‡]Maple Leaf International School−Tianjin TEDA, Tianjin 300457, China

Supporting Information

ABSTRACT: A new recycling way for simply recovered $LiCoO_2$ materials from spent Li-ion batteries (LIBs) is proposed to serve as a high-performance supercapacitor material in aqueous systems for the first time. A solvent method, using inexpensive DMF to recover the waste $LiCoO_2$ scraps, is suitable for industrial large-scale application with the prominent characteristics of low cost and simple technique. The recovered $LiCoO_2$ sample displays the maximum capacitances of 654 F g^{-1} with a capacity retention rate of 86.9% after 4000 cycles at 2 A g^{-1}. Excellent electrochemical capacitive behaviors demonstrate that the recovered $LiCoO_2$ material is a promising candidate for pseudocapacitors, which could overcome not only the serious resource waste and environment contamination of $LiCoO_2$ materials in spent LIBs but also the high-cost restriction of supercapacitor practical applications. So, it is hopeful for the recovered $LiCoO_2$ material to be used in supercapacitors, which has advantages of high power density, cost-effective, environment friendly and safe.

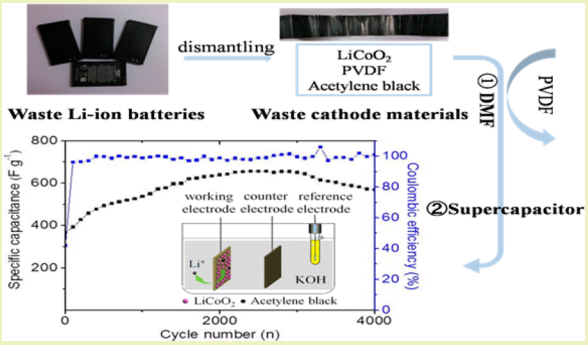

KEYWORDS: *Lithium cobalt oxide, Recovery, Solvent method, Spent lithium ion batteries, Supercapacitors*

INTRODUCTION

Li-ion batteries (LIBs) have accounted for more than 60% of worldwide sales in portable batteries since Sony made the first commercial cell in 1991, which can offer high energy density, flexibility, lightweight design and long lifespan.[1−4] But it is important to note that the organic electrolyte in LIBs is flammable and toxic HF can be released when the batteries burn. So, the irresponsible disposing of spent LIBs has become a potentially huge security problem. Though various new generation cathode materials ($LiMn_2O_4$, $LiNi_{0.33}Mn_{0.33}Co_{0.33}O_2$ and $LiFePO_4$) have been developed, $LiCoO_2$ is still the leading material for commercialized LIBs in laptops and cell phones.[5,6] And metal Li and Co are not renewable materials. The price of cobalt has exhibited a generally increasing trend since 2000[7] and has become the strong economic driver to focus on the recycling research of spent LIBs.

Currently, most of spent LIBs in cell phones and laptops are not recycled in time because this industry has poor economic benefit. But the consequent resource waste and environmental contamination cannot be neglected.[8] Many existing recovery systems are inclined to respectively recycle the metal of Co and Li from waste $LiCoO_2$ materials, which are still complex, environmentally unfriendly and expensive. Therefore, it is urgent to develop a simple and high profit method to recycle the waste $LiCoO_2$ material as a whole.

A solvent method is a simple, green and low-cost process to recover $LiCoO_2$ materials from spent LIBs, which is suitable for industrial large-scale application in environmental and economic considerations. Previous studies from our group have confirmed that the recovered $LiCoO_2$ materials can be used as anode materials for alkaline secondary batteries, which can deliver high energy densities but low power densities.[9−11] It is generally known that supercapacitors have attracted more attention because of their high-power density compared to batteries and fuel cells.[12−15] Herein the recovered $LiCoO_2$ samples have been proposed for a supercapacitor in an aqueous system to obtain high power densities for the first time. And if it is feasible, the recovered $LiCoO_2$ materials are promising to be explored for supercapacitors, which has advantages of high power density, cost-effective, environment friendly and safe.

As the excellent materials for electrochemical supercapacitor, Co-based metal oxides have been proved to possess well-defined redox activity and excellent electrochemical performances.[16−20] But high cost has become a restrictive factor for the reported Co-based materials. The approach to seek the resource-rich and low-cost candidate is effective to solve the above issue. The recovered $LiCoO_2$ materials used in a

Received: May 23, 2015
Revised: July 20, 2015
Published: August 7, 2015

DOI: 10.1021/acssuschemeng.5b00455
ACS Sustainable Chem. Eng. 2015, 3, 2435−2442

supercapacitor could overcome not only the serious resource waste and environment contamination of the $LiCoO_2$ materials in spent LIBs, but also the high-cost restriction of Co-based supercapacitor applications.

In this work, a new recycling way for the waste $LiCoO_2$ samples recovered through a solvent method is proposed to be used as a high-performance material in an aqueous supercapacitors system. And the commercial $LiCoO_2$ samples are also conducted for comparison to explore the electrochemical reaction mechanism.

EXPERIMENTAL SECTION

Recovery of $LiCoO_2$ from Spent LIBs. Commercial $LiCoO_2$ materials and spent LIBs (Prismatic Mobile Phone Batteries) are acquired from Tianjin B&M Science and Technology Joint-Stock Co. Ltd. A solvent method to recover $LiCoO_2$ sample from spent LIBs is shown in Figure 1.[11] $LiCoO_2$ cathode scraps with Al foil were obtained

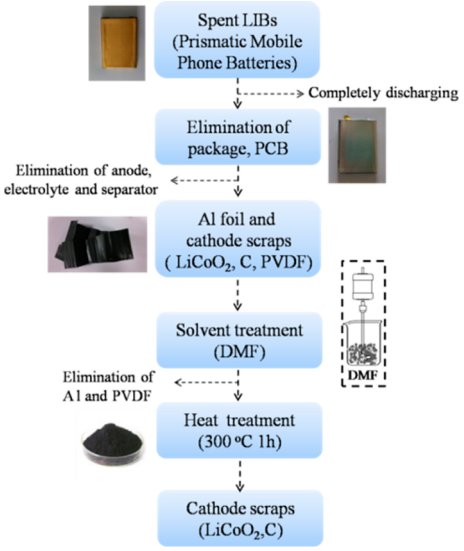

Figure 1. Flowsheet of solvent method for the recovered $LiCoO_2$ materials from spent LIBs.

through manually dismantling spent LIBs to remove both plastic gasket and steel cases. Then they were immediately placed in DMF organic solvent under fierce stirring to remove PVDF and Al foil. The obtained sediments were filtered with ethanol, dried at 80 °C in a vacuum and smashed by a 300 mesh screen to remove residual Al foil fragments. Subsequently, heat treatment (300 °C 1 h) was designed to restore the layer structure of recovered $LiCoO_2$ materials.

Compositional and Structural Characterization. The crystal structure and surface morphology of materials were characterized by X-ray diffraction (XRD, Rigaku MiniFlexII with Cu Kα radiation), scanning electron microscopy (SEM, SUPRA 55VP Field Emission). The elemental composition was measured by inductive coupled plasma atomic emission spectroscopy (ICP-AES, USA Themo Jarrel-Ash Corp), Fourier transform infrared spectroscopy (FTIR-650) and elemental analysis (EA, vario EL CUBE), and X-ray photoelectron spectroscopy (XPS, PHI5000 VersaProbe).

Electrochemical Measurements. For electrochemical measurements, the working electrodes were constructed by mixing the active material, acetylene black and polyvinylidene fluoride (PVDF) binder in a weight ratio of 80:10:10, which were dispersed in *N*-methyl-2-pyrrolidinone (NMP) solvent and ground thoroughly to form a slurry. Then the slurry was pressed at 20 MPa to a piece of nickel foam (1.0 cm × 1.0 cm) and dried under vacuum at 80 °C for 10 h. A nickel foam and an Hg/HgO reference electrode in 2 M KOH aqueous electrolyte were used as a counter electrode and reference electrode, respectively. The electrochemical measurements were conducted in a three compartment cell using a LAND battery test instrument (CT2001A). Cyclic voltammetry (CV) was conducted by a Zahner IM6e electrochemical workstation with voltage scan rates of 5, 10, 20 and 50 mV s^{-1}. The galvanostatic charge−discharge tests were conducted at the current densities of 1, 2, 5 and 10 A g^{-1}. Electrochemical impedance spectroscopy (EIS) measurements were carried out by applying an AC voltage with 5 mV amplitude in a frequency range from 0.01 Hz to 100 kHz at open circuit potential.

RESULT AND DISCUSSION

XRD patterns of the commercial and recovered $LiCoO_2$ samples are displayed in Figure 2a. It implies that all of

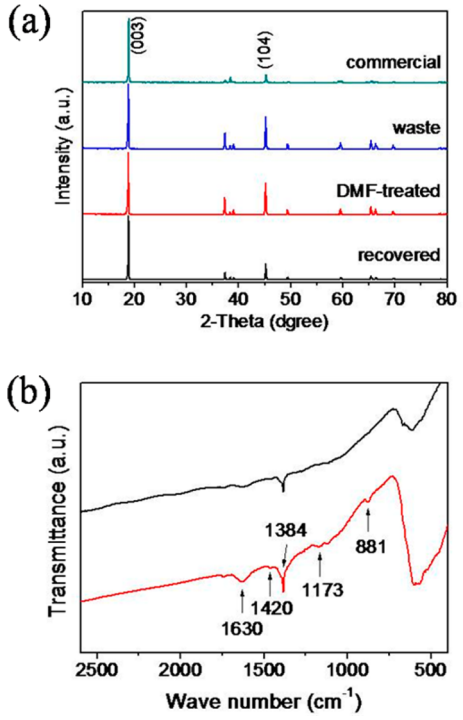

Figure 2. (a) XRD patterns of the commercial, waste, DMF-treated and recovered $LiCoO_2$ materials. (b) IR spectra of the waste and DMF-treated $LiCoO_2$ materials.

samples are highly purified without the peaks of impurities and Al foil in spent LIBs for the recovered $LiCoO_2$ materials has been completely removed through a solvent method (Figure 1). For the $LiCoO_2$ materials, a high ratio of I_{003}/I_{104} would indicate the improving of layer structure and the enhancement of electrochemical properties in alkaline electrolyte.[21,22] I_{003}/I_{104} values of the commercial, waste, DMF-treated and recovered $LiCoO_2$ materials are given in Table 1. The ratio value of waste $LiCoO_2$ materials reduces from 7.68 to 1.60, and it suggests that the intercalation/deintercalation of Li^+ has damaged the crystal form of $LiCoO_2$ materials during the

Table 1. I_{003}/I_{104} Value of the Commercial, Waste, DMF-Treated and Recovered $LiCoO_2$ Materials

$LiCoO_2$ material	I_{003}/I_{104}
commercial	7.68
waste	1.60
DMF-treated	0.95
recovered	3.41

DOI: 10.1021/acssuschemeng.5b00455
ACS Sustainable Chem. Eng. 2015, 3, 2435−2442

cycling of LIBs. And the I_{003}/I_{104} value of the DMF-treated $LiCoO_2$ samples is slightly decreased in comparison with waste $LiCoO_2$ materials, illustrating that solvent treatment process has also partly destroyed the layer structure of $LiCoO_2$ material. Therefore, a heat treatment process is proposed to restore the crystal form for the recovered $LiCoO_2$. To avoid a side reaction between $LiCoO_2$ and HF produced by the decomposing of PVDF, the heat temperature should be below 400 °C according to the TG curve of PVDF (Figure S1). Thus, the temperature of the heat process was chosen at 300 °C in this experiment. The I_{003}/I_{104} value for recovered $LiCoO_2$ materials obviously increased to 3.41 after heat treatment. The IR spectra of waste $LiCoO_2$ scraps before and after DMF treatment are shown in Figure 2b. Compared with the waste $LiCoO_2$ samples, the intensity of characteristic absorption peaks for PVDF (1630, 1420, 1173 and 881 cm^{-1}) in the DMF-treated $LiCoO_2$ materials is obviously decreased, indicating that most of PVDF in spent scraps is removed through a solvent method. The absorption peaks of 1384 cm^{-1} is assigned to the existing of NO_3^- from the impurity of KBr. Inductively coupled plasma (ICP) results demonstrate that mass content of $LiCoO_2$ in recovered material is 93.18%. It can be inferred that a small amount of conductive agent, binder and the surface coating layer, which is insensitive to DMF treatment, still remain in the recovered $LiCoO_2$ material.

The surface profiles and micromorphologies of the commercial and recovered $LiCoO_2$ samples are shown in Figure 3. SEM images illustrate that the recovered materials are

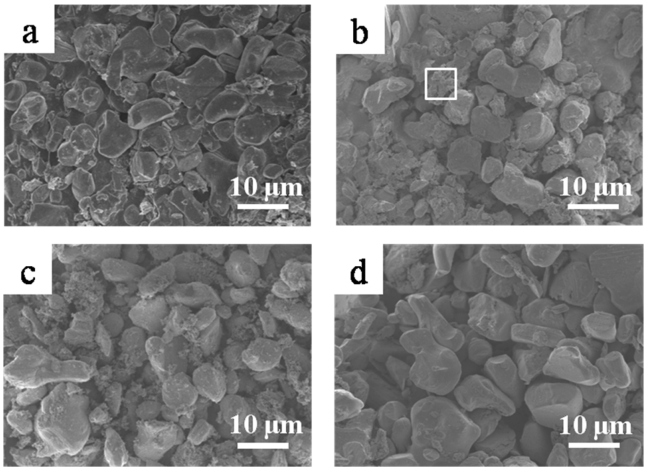

Figure 3. SEM patterns of the commercial (a), waste (b), DMF-treated (c) and recovered (d) $LiCoO_2$ samples.

composed of uniform particles with the size of 2−8 μm, which is similar to the commercial $LiCoO_2$ ones. Thus, we can infer that the particle size of recovered $LiCoO_2$ materials has little changes through a solvent method. The loose parts in white rectangle for the waste, DMF-treated and recovered $LiCoO_2$ materials are considered as acetylene black (Figure 3b−d). And its content is reduced visibly after heating process, which is consistent with the results of Element Analysis. The carbon contents of the waste, DMF-treated and recovered $LiCoO_2$ materials are 21.07%, 21.93% and 4.11%, respectively.

Electrochemical performances of $LiCoO_2$ electrodes were tested by performing continuous charge−discharge cycles at different current densities (Figure 4). The specific capacitance values of $LiCoO_2$ samples have been calculated from the applied charge/discharge current (i), mass of $LiCoO_2$ sample (m), discharge time (Δt) and operating potential (ΔV) using the following equation:[23]

$$C_s = \frac{i}{m(\Delta V/\Delta t)} \quad (1)$$

The commercial $LiCoO_2$ electrode exhibits the maximum specific capacitances of 936 F g^{-1} at 1 A g^{-1} in Figure 4a. High capacitances and good performance indicate that $LiCoO_2$ materials have great potential for supercapacitor applications. Discharge capacitances of the recovered $LiCoO_2$ electrodes are slightly lower, which could attribute to the existence of residual PVDF and the damage of crystal form. However, the recovered $LiCoO_2$ samples show the outstanding cycling stability with a capacity retention rate of more than 93% after 2000 cycles. The superior performance can be explained as the synergistic effect between carbon material and active materials.[24−30] Specific capacitances of the commercial and recovered $LiCoO_2$ samples at different current densities are presented in Figure 4b. For the recovered $LiCoO_2$ electrode, the specific capacitances of 730, 657, 451 and 190 F g^{-1} at the current densities of 1, 2, 5 and 10 A g^{-1} are obtained. The capacitance decrease corresponding to the increase of the discharge current density likely results from the increase of the potential drop (iR) and the relatively insufficient Faradaic redox reaction of the active material under higher discharge current densities. Fortunately, Compared with the reported Co_3O_4 materials,[31,32] the discharge capacities and rate capabilities of recovered $LiCoO_2$ samples are attractive. For example, Li et al. reported that 3D hierarchical Co_3O_4 spheres displayed the capacitances of 754 F g^{-1} at 1 A g^{-1} for supercapacitors.[16] Lu et al. synthesized the cobalt oxide aerogels with the pseudocapacitances of more than 600 F g^{-1} at 1 mg cm^{-2}.[33] Lou et al. reported the porous Co_3O_4 nanowires for supercapacitors and it exhibited a specific capacitance of 171 F g^{-1} at 15 A g^{-1}.[17] The outstanding capacitance values suggest that the $LiCoO_2$ electrodes have a good rate capability, which is a very important parameter to estimate the electrode materials for supercapacitors.

Cyclic life and energy deliverable efficiency of the recovered $LiCoO_2$ electrode at a current density of 2 A g^{-1} are shown in Figure 4c. The sample displays the maximum capacitances of 654 F g^{-1} with an excellent capacity retention rate of 86.9% after 4000 cycles. The Coulombic efficiency of nearly 100% indicates the excellent long-term electrochemical stability. The decrease of discharge capacitance could result from the consumption of electrolyte, caused by the irreversible reaction between electrode materials and electrolyte. In addition, the galvanostatic charge−discharge curves of the recovered materials are shown in Figure 4d, indicating that the $LiCoO_2$ electrodes possess highly reversible charge−discharge course and excellent electrochemical capacitive behavior.

CV measurements were performed at sweep rates of 5, 10, 20 and 50 mV s^{-1} in a fixed potential range of 0−0.6 V (versus Hg/HgO) for the commercial and recovered $LiCoO_2$ samples in Figure 5a,b. One pair of redox peaks over the entire range of scan rates is clearly observed. The capacitive characteristic is very distinct from that of the typical electric double-layer capacitors (EDLC) in which the CV curves should assume a nearly rectangular shape.[34−37] The oxidation peak currents are also increased with the rising of scan rates, which suggests the good reversibility of the fast charge−discharge response for active materials. The comparison of the sample signal from $LiCoO_2$ to background signal from Ni foam and acetylene black

DOI: 10.1021/acssuschemeng.5b00455
ACS Sustainable Chem. Eng. 2015, 3, 2435−2442

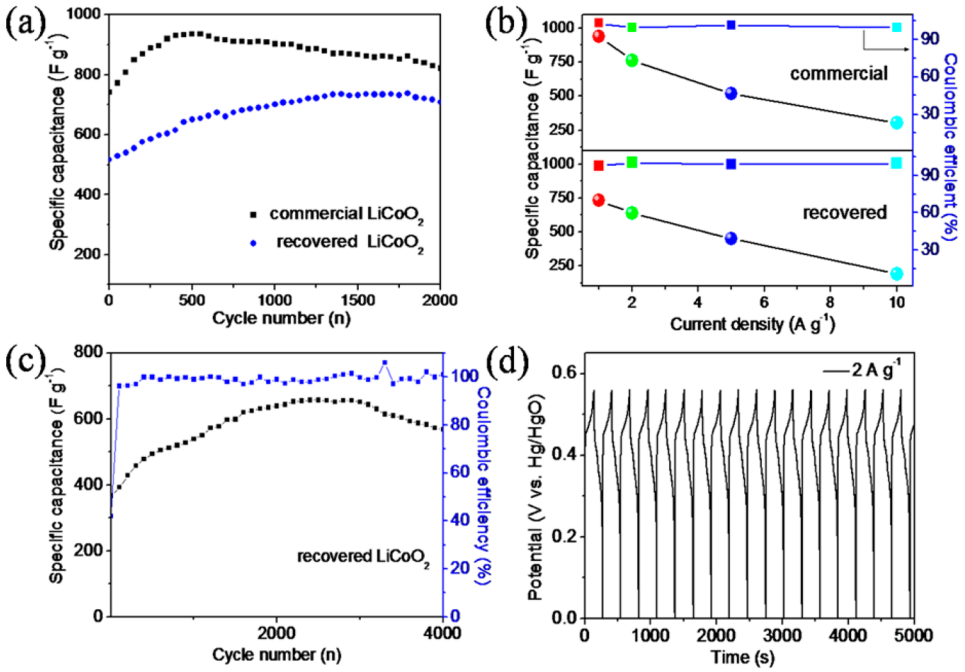

Figure 4. (a) Electrochemical capacitance of the commercial and recovered $LiCoO_2$ materials at a current density of 1 A g^{-1}. (b) Rate performance of the commercial and recovered $LiCoO_2$ samples at various discharge current densities. (c) Discharge specific capacitance and Coulombic efficiency of the recovered $LiCoO_2$ samples after 4000 cycles at 2 A g^{-1}. (d) Galvanostatic charge−discharge voltage profiles of the recovered $LiCoO_2$ electrode at a current density of 2 A g^{-1}.

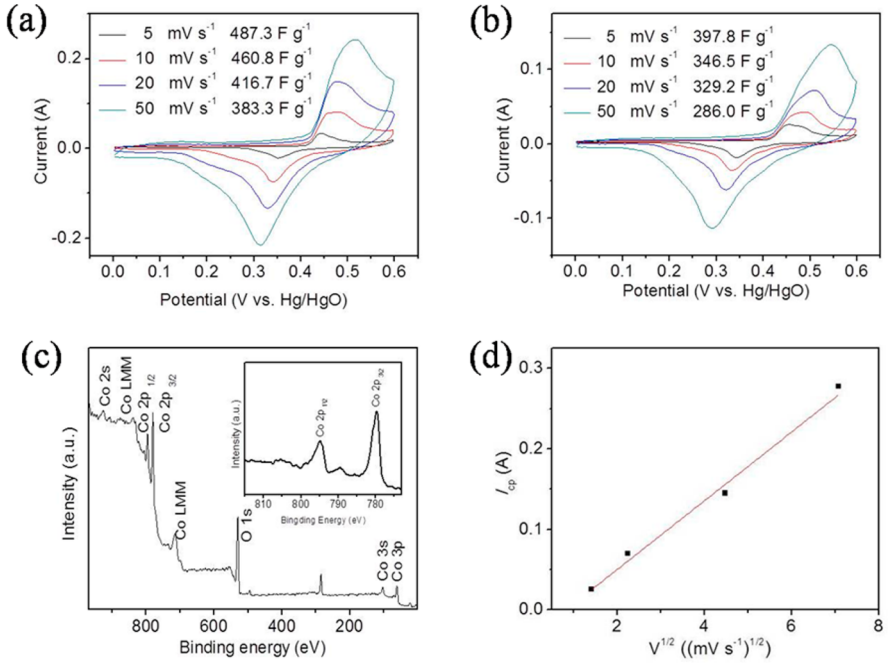

Figure 5. CV curves of the commercial (a) and recovered $LiCoO_2$ (b) electrodes at scan rates of 5, 10, 20 and 50 mV s^{-1}. (c) XPS spectrum of the recovered $LiCoO_2$ material after 2000 charge−discharge cycles. (d) Relationship between the cathodic peak current (I_{pc}) and the square root of the scan rate ($\nu^{1/2}$).

are shown in Figure S2. It is noted that background signal derived from Ni foam and acetylene black is very low (about 5.63% and 6.25%). The pair of weak redox peaks of Ni foam without active materials may be attributed to the transformation between Ni(II) and Ni(III) due to the surface passivation of Ni in alkaline electrolyte. And the contribution of acetylene black in the recovered $LiCoO_2$ materials for discharge capacitances can be neglected. Therefore, the capacitance is mainly attributed to the $LiCoO_2$ material.

From XPS spectrum of the recovered $LiCoO_2$ materials after 2000 charge−discharge cycles, the peaks (inset in Figure 5c) located at 779.8 and 794.9 eV are assigned to the binding energy of Co $2p_{3/2}$ and Co $2p_{1/2}$, indicating the existing of Co^{3+}. But the tetravalent Co cannot be detected because of high oxidation state and instability. The lithium content in

DOI: 10.1021/acssuschemeng.5b00455
ACS Sustainable Chem. Eng. 2015, 3, 2435−2442

alkaline electrolyte is 5.71 μg mL^{-1} after 2000 cycles by ICP-AES test, demonstrating that parts of lithium in the $LiCoO_2$ electrode are dissolved in KOH aqueous solution in the form of Li^+ upon the cycling.[9] It further confirms that electrochemical reaction on the $LiCoO_2$ electrode can be attributed to the conversion between Co(III) and Co(IV).

The specific capacitance (C_s) values of the recovered $LiCoO_2$ samples estimated from CV curves were 397.8, 346.5, 329.2 and 286.0 F g^{-1} at scan rates of 5, 10, 20 and 50 mV s^{-1}, respectively, calculated by the following equation:[41]

$$C_s = \frac{1}{\upsilon w(V_a - V_c)} \int_{V_a}^{V_c} IV\,dV \quad (2)$$

The C_s values are calculated graphically by integrating the area under the $I-V$ curves and then dividing by the sweep rate υ (V s^{-1}), the mass of $LiCoO_2$ (w), and the potential window (V_a to V_c). Similarly, the specific capacitances for the commercial $LiCoO_2$ samples are 487.3, 460.8, 416.7 and 383.3 F g^{-1} at the same scan rates. An almost linear/quasi-linear relationship for the recovered $LiCoO_2$ electrode has been observed between anodic peak current density and applied scan rate, as shown in Figure 5d, which indicates the reactions in the system are controlled by the diffusion process and surface redox reactions taking place in charge storage process.[42]

Figure 6a shows the discharge curves of the recovered $LiCoO_2$ electrode measured at various current densities of 1, 2, 5 and 10 A g^{-1}. And the nonlinearity of the discharge curve is characteristic of pseudocapacitance behavior due to electrochemical quasi-reversible redox reactions at the electrode–electrolyte interface. The linear potential variation in the nonlinear discharge curve from 0.0 to ~0.32 V indicates the double layer capacitance behavior whereas the variation of potential from ~0.32 to 0.5 V represents pure pseudocapacitance behavior.[43−45] And the discharge curves of the commercial $LiCoO_2$ samples were also performed at same current densities in Figure S3 to testify the electrochemical behaviors. Initial charge–discharge cycles for the recovered $LiCoO_2$ samples as well as the corresponding duration of charging and discharging at 1 A g^{-1} are not entirely symmetrical in Figure 6b. And the Coulombic efficiency η of charge storage process is a measure for the competence of charge/ion transfer during an electrochemical reaction:

$$\eta = \frac{t_d}{t_c} \times 100 \quad (3)$$

where t_d and t_c are the discharge and charge times, respectively. The Coulombic efficiency values of the first cycle are undesired at current densities of 1, 2, 5 and 10 A g^{-1}, but the derived values (η) of the subsequent second cycle for the recovered $LiCoO_2$ electrode can reach 87.6%, 89.5%, 91.7% and 93.8% (Figure 6c), respectively. And the Coulombic efficiency η is almost close to ~100% after 400 cycles due to the gradual surface activation of cyclic process.

Because of the dominating effect of the ions and electron transport kinetic features in electrodes as well as at the electrode/electrolyte interface on the pseudocapacitance performance, lower internal resistance (higher conductivity) is significant, for less energy will be wasted during charge storage process.[43] The Nyquist plots of the $LiCoO_2$ electrodes in the frequency range of 0.01–10^5 Hz are shown in Figure 7a to evaluate quantitatively their intrinsic resistance and relative electrochemical performance. The impedance characteristics

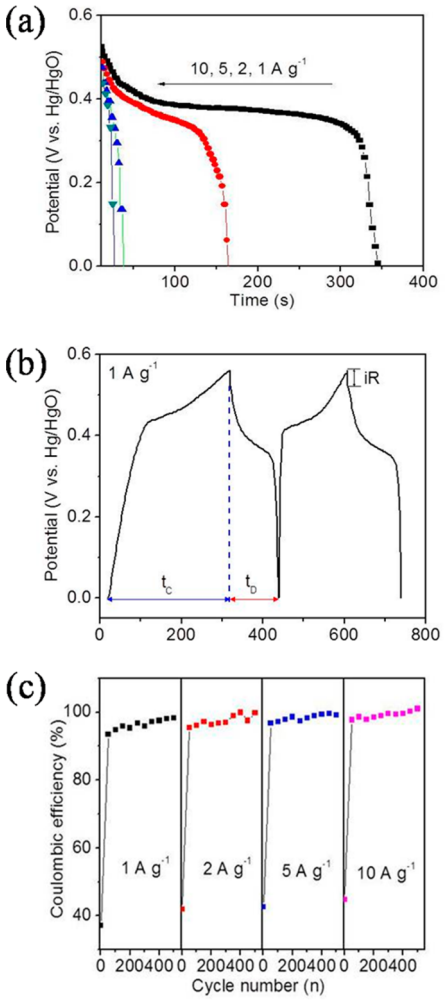

Figure 6. (a) Charge–discharge curves of the recovered $LiCoO_2$ sample at different current densities. (b) Initial charge–discharge curves of the recovered sample at a current density of 1 A g^{-1} (t_c and t_d represents charging and discharging time, respectively. iR represents the corresponding voltage drops). (c) Coulombic efficiency (η) derived from charge–discharge cycles of the recovered $LiCoO_2$ samples at various current densities of 1, 2, 5 and 10 A g^{-1}.

were analyzed by the CNLS fitting method based on a Randles equivalent circuit, as depicted below:[46,47] where R_s and R_{ct} are

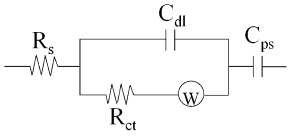

solution and charge-transfer resistances, respectively. C_{dl} and C_{ps} in the circuit represent double layer and pseudocapacitance, respectively. The interfacial diffusive resistance (Warburg impedance) in the process has been designated as "W".

Two major characteristic features at the high and low frequency regions are attributed to various resistance phenomena during different interfacial processes in Faradaic reactions. The semicircle at high frequency is characteristic of the resistance at the solid oxide/liquid electrolyte interface due to discontinuity in the charge transfer process, which is a result of the different conductivities between solid oxide (electronic conductivity) and aqueous electrolyte phase (ionic conductiv-

DOI: 10.1021/acssuschemeng.5b00455
ACS Sustainable Chem. Eng. 2015, 3, 2435–2442

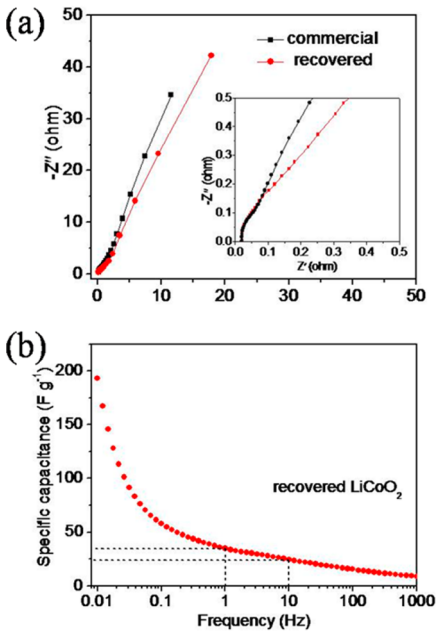

Figure 7. (a) Complex plane impedance plots (Nyquist plots) of the commercial and recovered $LiCoO_2$ samples. (b) Frequency dependent specific capacitance values of the recovered $LiCoO_2$ samples, derived from impedance measurements samples.

ity). From an enlarged view of the semicircles at high frequency in the inset, charge-transfer resistances (R_{ct}) induced by the redox reaction for the commercial and recovered $LiCoO_2$ samples are nearly identical. The near linear EIS plots of the $LiCoO_2$ samples in the lower frequency region are characteristic of Warburg impedance, *W*, where the resistance behavior can be attributed to diffusion of the OH^- ion on the electrode surface. The more vertical line leaning to imaginary axis indicates the more facile electrolyte diffusion to the surface and the more ideal capacitor behavior of active material. The low-slope straight line of the recovered $LiCoO_2$ sample, compared to commercial sample, demonstrates high diffusion resistance resulting from the existence of residual PVDF and the damage of crystal form as we mentioned. The rate response of the $LiCoO_2$ samples has been further verified from the capacitor response frequency:[48,49] the frequency where $\Phi = -45°$ ($f_{\Phi=-45}$) in the $f-\Phi$ plot in Figure S4. The marginally lower capacitor response frequency of the recovered $LiCoO_2$ electrode indicates slightly faster response time and lower discharge capacitances in comparison with the commercial one.

The experimental impedance data of recovered $LiCoO_2$ sample was converted to specific capacitance (C_s) using the following equation:[44,50]

$$C_s = \frac{1}{2\pi f Z''} \quad (4)$$

and plotted against frequency *f*, as shown in Figure 7b. The specific capacitance values inevitably decrease in the entire frequency region. The recovered $LiCoO_2$ electrodes display specific capacitance values of 34.7 F g^{-1} at 1 Hz and 25.1 F g^{-1} at 10 Hz.

CONCLUSIONS

In summary, a $LiCoO_2$ material recovered from a solvent method was used as a high-performance pseudocapacitive material in an aqueous system for the first time. High capacitances and good performance indicate that $LiCoO_2$ materials have great potential for supercapacitor applications. The sample displays the maximum discharge capacitance of 654 F g^{-1} with Coulombic efficiency of nearly 100% and a capacity retention rate of 86.9% after 4000 cycles at 2 A g^{-1}. Electrochemical stability at higher current rates and low ESR values from impedance measurements show good utility value of the recovered $LiCoO_2$ material in fabricating a wide range of electrochemical supercapacitors. The excellent results show the promise for the recovered $LiCoO_2$ material in supercapacitors with the merit of high power density, cost-effective, environment friendly and safe.

ASSOCIATED CONTENT

Supporting Information

The Supporting Information is available free of charge on the ACS Publications website at DOI: 10.1021/acssuschemeng.5b00455.

TG-DTG curve of PVDF, CV curves of acetylene black, recovered $LiCoO_2$ material and Ni foam without loading of active materials at the scan rate of 5 mV s^{-1}, discharge curves of the commercial $LiCoO_2$ samples at different current densities, frequency dependence of the phase angle, Φ, for the commercial and recovered $LiCoO_2$ samples (PDF).

AUTHOR INFORMATION

Corresponding Author

*Y. Wang. Tel.: +86 22 23503639. Fax: +86 22 23503639. E-mail: wangyj@nankai.edu.cn.

Notes

The authors declare no competing financial interest.

ACKNOWLEDGMENTS

This work was financially supported by 973 (2011CB935900), NSFC (51471089), MOE (IRT13R30), 111 Project (B12015), Research Fund for the Doctoral Program of Higher Education of China (20120031110001), Tianjin Sci & Tech Project (10SYSYJC27600).

REFERENCES

(1) Armand, M.; Tarascon, J. Building better batteries. *Nature* **2008**, *451*, 652−657.

(2) Yin, Z.; Fan, W.; Ding, Y.; Li, J.; Guan, L.; Zheng, Q. Shell Structure control of PPy-modified CuO composite nanoleaves for lithium batteries with improved cyclic performance. *ACS Sustainable Chem. Eng.* **2015**, *3*, 507−517.

(3) Etacheri, V.; Marom, R.; Elazari, R.; Salitra, G.; Aurbach, D. Challenges in the development of advanced Li-ion batteries: a review. *Energy Environ. Sci.* **2011**, *4*, 3243−3262.

(4) Kang, K. S.; Meng, Y. S.; Breger, J.; Grey, C. P.; Ceder, G. Electrodes with high power and high capacity for rechargeable lithium batteries. *Science* **2006**, *311*, 977−980.

(5) Rui, X.; Zhao, X.; Lu, Z.; Tan, H.; Sim, D.; Hng, H. H.; Yazami, R.; Lim, T. M.; Yan, Q. Olivine-type nanosheets for lithium Ion battery cathodes. *ACS Nano* **2013**, *7*, 5637−5646.

(6) Ji, H.; Miao, X.; Wang, L.; Qian, B.; Yang, G. Effects of microwave-hydrothermal conditions on the purity and electrochemical performance of orthorhombic $LiMnO_2$. *ACS Sustainable Chem. Eng.* **2014**, *2*, 359−366.

(7) Li, L.; Dunn, J. B.; Zhang, X. X.; Gaines, L.; Chen, R. J.; Wu, F.; Amine, K. Recovery of metals from spent lithium-ion batteries with organic acids as leaching reagents and environmental assessment. *J. Power Sources* **2013**, *233*, 180−189.

DOI: 10.1021/acssuschemeng.5b00455
ACS Sustainable Chem. Eng. 2015, 3, 2435−2442

(8) Luo, X.; Guo, B.; Luo, J.; Deng, F.; Zhang, S.; Luo, S.; Crittenden, J. Recovery of lithium from waste water using development of Li ion-imprinted polymers. *ACS Sustainable Chem. Eng.* **2015**, *3*, 460−467.
(9) Song, D.; Xu, Y.; An, C.; Wang, Q.; Wang, Y.; Li, L.; Wang, Y.; Jiao, L.; Yuan, H. Recovered $LiCoO_2$ as anode materials for Ni/Co power batteries. *Phys. Chem. Chem. Phys.* **2012**, *14*, 71−75.
(10) Xu, Y.; Song, D.; Li, J.; Li, L.; An, C.; Wang, Y.; Jiao, L.; Yuan, H. Electrochemical properties of $LiCoO_2$+x% S mixture as anode material for alkaline secondary battery. *Electrochim. Acta* **2012**, *85*, 352−357.
(11) Xu, Y.; Song, D.; Li, L.; An, C.; Wang, Y.; Jiao, L.; Yuan, H. A simple solvent method for the recovery of Li_xCoO_2 and its applications in alkaline rechargeable batteries. *J. Power Sources* **2014**, *252*, 286−291.
(12) Hall, P. J.; Mirzaeian, M.; Fletcher, S. I.; Sillars, F. B.; Rennie, A. J. R.; Shitta-Bey, G. O.; Wilson, G.; Cruden, A.; Carter, R. Energy storage in electrochemical capacitors: designing functional materials to improve performance. *Energy Environ. Sci.* **2010**, *3*, 1238−1251.
(13) Wang, G.; Zhang, L.; Zhang, J. A review of electrode materials for electrochemical supercapacitors. *Chem. Soc. Rev.* **2012**, *41*, 797−828.
(14) Zhi, M.; Xiang, C.; Li, J.; Li, M.; Wu, N. Nanostructured carbon-metal oxide composite electrodes for supercapacitors: a review. *Nanoscale* **2013**, *5*, 72−88.
(15) Vijayakumar, S.; Nagamuthu, S.; Muralidharan, G. Porous NiO/C Nanocomposites as electrode material for electrochemical supercapacitors. *ACS Sustainable Chem. Eng.* **2013**, *1*, 1110−1118.
(16) Xiao, Y.; Liu, S.; Li, F.; Zhang, A.; Zhao, J.; Fang, S.; Jia, D. 3D Hierarchical Co_3O_4 Twin-Spheres with an Urchin-Like Structure: Large-scale synthesis, multistep-splitting growth, and electrochemical pseudocapacitors. *Adv. Funct. Mater.* **2012**, *22*, 4052−4059.
(17) Wang, B.; Zhu, T.; Wu, H. B.; Xu, R.; Chen, J. S.; Lou, X. W. Porous Co_3O_4 nanowires derived from long $Co(CO_3)_{0.5}(OH)\cdot 0.11H_2O$ nanowires with improved supercapacitive properties. *Nanoscale* **2012**, *4*, 2145−2149.
(18) Chen, K.; Yang, Y.; Li, K.; Ma, Z.; Zhou, Y.; Xue, D. $CoCl_2$ Designed as excellent pseudocapacitor electrode materials. *ACS Sustainable Chem. Eng.* **2014**, *2*, 440−444.
(19) Wang, L.; Dong, Z.; Wang, Z.; Zhang, F.; Jin, J. Layered α-$Co(OH)_2$ nanocones as electrode materials for pseudocapacitors: understanding the Effect of interlayer space on electrochemical activity. *Adv. Funct. Mater.* **2013**, *23*, 2758−2764.
(20) Ghosh, D.; Giri, S.; Das, C. K. Preparation of CTAB-assisted hexagonal platelet $Co(OH)_2$/graphene hybrid composite as efficient supercapacitor electrode material. *ACS Sustainable Chem. Eng.* **2013**, *1*, 1135−1142.
(21) Li, L.; Chen, R.; Sun, F.; Wu, F.; Liu, J. Preparation of $LiCoO_2$ films from spent lithium-ion batteries by a combined recycling process. *Hydrometallurgy* **2011**, *108*, 220−225.
(22) Gan, Y.; Zhang, L.; Wen, Y.; Wang, F.; Su, H. Carbon combustion synthesis of lithium cobalt oxide as cathode material for lithium ion battery. *Particuology* **2008**, *6*, 81−84.
(23) Xiong, S.; Yuan, C.; Zhang, X.; Xi, B.; Qian, Y. Controllable Synthesis of mesoporous Co_3O_4 nanostructures with tunable morphology for application in supercapacitors. *Chem. - Eur. J.* **2009**, *15* (21), 5320−5326.
(24) Wu, Z.; Zhou, G.; Yin, L.; Ren, W.; Li, F.; Cheng, H. Graphene/metal oxide composite electrode materials for energy storage. *Nano Energy* **2012**, *1* (1), 107−131.
(25) Wang, H.; Casalongue, H.; Liang, Y.; Dai, H. $Ni(OH)_2$ Nanoplates grown on graphene as advanced electrochemical pseudocapacitor materials. *J. Am. Chem. Soc.* **2010**, *132*, 7472−7477.
(26) Wang, H.; Holt, C.; Li, Z.; Tan, X.; Amirkhiz, B.; Xu, Z.; Olsen, B.; Stephenson, T.; Mitlin, D. Graphene-nickel cobaltite nanocomposite asymmetrical supercapacitor with commercial level mass loading. *Nano Res.* **2012**, *5*, 605−617.
(27) Han, Y.; Wang, Y.; Wang, Y.; Jiao, L.; Yuan, H.; Liu, S. Hydrothermal synthesis and electrochemical properties of cobalt-carbon nanotubes nanocomposite. *Electrochim. Acta* **2011**, *56*, 3258−3263.
(28) Li, L.; Xu, Y.; An, C.; Wang, Y.; Jiao, L.; Yuan, H. Enhanced electrochemical properties of Co/CMK-3 composite as negative material for alkaline secondary battery. *J. Power Sources* **2013**, *238*, 117−122.
(29) Du, H.; Jiao, L.; Wang, Q.; Peng, W.; Song, D.; Wang, Y.; Yuan, H. Structure and electrochemical properties of ball-milled Co-carbon nanotube composites as negative electrode material of alkaline rechargeable batteries. *J. Power Sources* **2011**, *196*, 5751−5755.
(30) Xin, S.; Guo, Y.; Wan, L. Nanocarbon networks for advanced rechargeable lithium batteries. *Acc. Chem. Res.* **2012**, *45* (10), 1759−1769.
(31) Zhu, T.; Chen, J. S.; Lou, X. W. Shape-controlled synthesis of porous Co_3O_4 nanostructures for application in supercapacitors. *J. Mater. Chem.* **2010**, *20*, 7015−7020.
(32) Kim, Y.; Cha, S.; Hong, S. Nanoporous cobalt foam and a Co/$Co(OH)_2$ core-shell structure for electrochemical applications. *J. Mater. Chem. A* **2013**, *1*, 9802−9808.
(33) Wei, T.; Chen, C.; Chang, K.; Lu, S.; Hu, C. Cobalt oxide aerogels of ideal supercapacitive properties prepared with an epoxide synthetic route. *Chem. Mater.* **2009**, *21* (14), 3228−3233.
(34) Liu, C.; Yu, Z.; Neff, D.; Zhamu, A.; Jang, B. Graphene-based supercapacitor with an ultrahigh energy density. *Nano Lett.* **2010**, *10*, 4863−4868.
(35) Brownson, D. A. C.; Kampouris, D. K.; Banks, C. An overview of graphene in energy production and storage applications. *J. Power Sources* **2011**, *196*, 4873−4885.
(36) Zhu, Y.; Murali, S.; Stoller, M.; Ganesh, K.; Cai, W.; Ferreira, P.; Pirkle, A.; Wallace, R.; Cychosz, K.; Thommes, M.; Su, D.; Stach, E.; Ruoff, R. Carbon-based supercapacitors produced by activation of graphene. *Science* **2011**, *332*, 1537−1541.
(37) Futaba, D.; Hata, K.; Yamada, T.; Hiraoka, T.; Hayamizu, Y.; Kakudate, Y.; Tanaike, O.; Hatori, H.; Yumura, M.; Iijima, S. Shape-engineerable and highly densely packed single-walled carbon nanotubes and their application as supercapacitor electrodes. *Nat. Mater.* **2006**, *5*, 987−994.
(38) Wang, Q.; Jiao, L.; Du, H.; Yang, J.; Huan, Q.; Peng, W.; Si, Y.; Wang, Y.; Yuan, H. Facile synthesis and superior supercapacitor performances of three-dimensional cobalt sulfide hierarchitectures. *CrystEngComm* **2011**, *13*, 6960−6963.
(39) Yuan, C.; Yang, L.; Hou, L.; Shen, L.; Zhang, X.; Lou, X. Growth of ultrathin mesoporous Co_3O_4 nanosheet arrays on Ni foam for high-performance electrochemical capacitors. *Energy Environ. Sci.* **2012**, *5*, 7883−7887.
(40) Li, M.; Xu, S.; Liu, T.; Wang, F.; Yang, P.; Wang, L.; Chu, P. Electrochemically-deposited nanostructured $Co(OH)_2$ flakes on three-dimensional ordered nickel/silicon microchannel plates for miniature supercapacitors. *J. Mater. Chem. A* **2013**, *1*, 532−540.
(41) Meher, S.; Rao, G. Ultralayered Co_3O_4 for high-erformance supercapacitor Applications. *J. Phys. Chem. C* **2011**, *115*, 15646−15654.
(42) Xiao, Y.; Zhang, A.; Liu, S.; Zhao, J.; Fang, S.; Jia, D.; Li, F. Free-standing and porous hierarchical nanoarchitectures constructed with cobalt cobaltite nanowalls for supercapacitors with high specific capacitances. *J. Power Sources* **2012**, *219*, 140−146.
(43) Meher, S.; Rao, G. Effect of microwave on the nanowire morphology, optical, magnetic, and pseudocapacitance behavior of Co_3O_4. *J. Phys. Chem. C* **2011**, *115*, 25543−25556.
(44) Meher, S.; Justin, P.; Ranga Rao, G. Nanoscale morphology dependent pseudocapacitance of NiO: influence of intercalating anions during synthesis. *Nanoscale* **2011**, *3*, 683−692.
(45) Sugimoto, W.; Iwata, H.; Yasunaga, Y.; Murakami, Y.; Takasu, Y. Preparation of ruthenic acid nanosheets and utilization of its interlayer surface for electrochemical energy storage. *Angew. Chem., Int. Ed.* **2003**, *42*, 4092−4096.
(46) Wei, T.; Chen, C.; Chang, K.; Lu, S.; Hu, C. Cobalt oxide aerogels of ideal supercapacitive properties prepared with an epoxide synthetic route. *Chem. Mater.* **2009**, *21*, 3228−3233.
(47) Hsu, Y.; Chen, Y.; Lin, Y.; Chen, L.; Chen, K. Reversible phase transformation of MnO_2 nanosheets in an electrochemical capacitor

DOI: 10.1021/acssuschemeng.5b00455
ACS Sustainable Chem. Eng. 2015, 3, 2435−2442

investigated by in situRaman spectroscopy. *Chem. Commun.* **2011**, *47*, 1252−1254.
(48) Sugimoto, W.; Iwata, H.; Yokoshima, K.; Murakami, Y.; Takasu, Y. Proton and electron conductivity in hydrous ruthenium oxides evaluated by electrochemical impedance spectroscopy: the origin of large capacitance. *J. Phys. Chem. B* **2005**, *109*, 7330−7338.
(49) Lin, K.; Chang, K.; Hu, C.; Li, Y. Mesoporous RuO_2 for the next generation supercapacitors with an ultrahigh power density. *Electrochim. Acta* **2009**, *54*, 4574−4581.
(50) Justin, P.; Meher, S.; Rao, G. Tuning of capacitance behavior of NiO using anionic, cationic, and nonionic surfactants by hydrothermal synthesis. *J. Phys. Chem. C* **2010**, *114*, 5203−5210.

DOI: 10.1021/acssuschemeng.5b00455
ACS Sustainable Chem. Eng. 2015, 3, 2435−2442